Nuclear matter Properties and Neutron Star Phenomenology Using the Finite Range Simple Effective Interaction

X. Viñas[a,b] et al.

[a]Universitat de Barcelona, Barcelona, Spain [b]Institut Menorquí d'Estudis, Maó, Spain

QNP, Barcelona, July 9th, 2024

X. Viñas et al., Symmetry 16, 215 (2024) and references therein

The Simple Efffective Interaction (SEI)

The finite range simple effective interaction was initially proposed by Behera and collaborators and has the following explicit form for a Yukawa finite range form factor (SEI-Y),

$$\begin{aligned} V_{eff} &= t_0(1+x_0P_\sigma)\delta(\vec{r}) + \frac{t_3}{6}(1+x_3P_\sigma)\left(\frac{\rho(\vec{R})}{1+b\rho(\vec{R})}\right)^\gamma \delta(\vec{r}) \\ &+ (W + BP_\sigma - HP_\tau - MP_\sigma P_\tau)\frac{e^{-r/\alpha}}{r/\alpha} + \text{Spin-orbit part} \end{aligned}$$

where a zero-range spin-orbit (SO) interaction depending on a strength parameter W_0 is taken to deal with finite nuclei. The SEI in Eq.(**??**) has 12 parameters in total, namely, $\alpha, \gamma, b, x_0, x_3, t_0, t_3, W, B, H,$ and M plus the spin-orbit strength parameter W_0, which enters in the description of finite nuclei.

Nine of these twelve parameters are fitted to reproduce empirical constraints and microscopical results in nuclear nd neutron matter.

SEI in asymmetric nuclear matter

$$H_T(\rho_n,\rho_p)=\frac{\hbar^2}{2m}\int\left[f_T^n(\mathbf{k})+f_T^p(\mathbf{k})\right]k^2d^3k$$
$$+\frac{1}{2}\left[\frac{\varepsilon_0^I}{\rho_0}+\frac{\varepsilon_\gamma^I}{\rho_0^{\gamma+1}}\left(\frac{\rho}{1+b\rho}\right)^\gamma\right]\left(\rho_n^2+\rho_p^2\right)+\left[\frac{\varepsilon_0^{uI}}{\rho_0}+\frac{\varepsilon_\gamma^{uI}}{\rho_0^{\gamma+1}}\left(\frac{\rho}{1+b\rho}\right)^\gamma\right]\rho_n\rho_p$$
$$+\frac{\varepsilon_{ex}^I}{2\rho_0}\int\int\left[f_T^n(\mathbf{k})f_T^n(\mathbf{k}')+f_T^p(\mathbf{k})f_T^p(\mathbf{k}')\right]g\left(|\mathbf{k}-\mathbf{k}'|\right)d^3kd^3k'$$
$$+\frac{\varepsilon_{ex}^{uI}}{2\rho_0}\int\int\left[f_T^n(\mathbf{k})f_T^p(\mathbf{k}')+f_T^p(\mathbf{k})f_T^n(\mathbf{k}')\right]g\left(|\mathbf{k}-\mathbf{k}'|\right)d^3kd^3k',$$

$$g_Y(|\mathbf{k}-\mathbf{k}'|)=(\mathbf{1}+((\mathbf{k}-\mathbf{k}')/\mathbf{\Lambda})^2)^{-1}\quad \mathbf{g_G}(|(\mathbf{k}-\mathbf{k}')|)=\mathbf{e}^{-\frac{(\mathbf{k}-\mathbf{k}')}{\mathbf{\Lambda}})^2},$$

$$f_T^{n(p)}(\vec{k})=1+exp\left[\left\{\epsilon_T^{n(p)}(k,\rho_n,\rho_p)-\mu_T^{n(p)}\right\}/T\right]^{-1}$$

$$\epsilon_T^{n(p)}(\mathbf{k},\rho_n,\rho_p)=\frac{\hbar^2k^2}{2m}+u_T^{n(p)}(\mathbf{k},\rho_n,\rho_p)$$

$$
\begin{aligned}
H_Y(\rho_n,\rho_p) &= \frac{3\hbar^2}{10m}(k_n^2\rho_n + k_p^2\rho_p) + \frac{\varepsilon_0^l}{2\rho_0}(\rho_n^2+\rho_p^2) + \frac{\varepsilon_0^{ul}}{\rho_0}\rho_n\rho_p \\
&+ \left[\frac{\varepsilon_\gamma^l}{2\rho_0^{\gamma+1}}(\rho_n^2+\rho_p^2) + \frac{\varepsilon_\gamma^{ul}}{\rho_0^{\gamma+1}}\rho_n\rho_p\right]\left(\frac{\rho(\mathbf{R})}{1+b\rho(\mathbf{R})}\right)^\gamma \\
&+ \frac{\varepsilon_{ex}^l}{2\rho_0}\left[\rho_n^2\left[\left(\frac{3\Lambda^6}{32k_n^6}+\frac{9\Lambda^4}{8k_n^4}\right)\ln\left(1+\frac{4k_n^2}{\Lambda^2}\right) - \frac{3\Lambda^4}{8k_n^4} + \frac{9\Lambda^2}{4k_n^2} - \frac{3\Lambda^3}{k_n^3}\tan^{-1}\left(\frac{2k_n}{\Lambda}\right)\right]\right] \\
&+ \frac{\varepsilon_{ex}^l}{2\rho_0}\left[\rho_p^2\left[\left(\frac{3\Lambda^6}{32k_p^6}+\frac{9\Lambda^4}{8k_p^4}\right)\ln\left(1+\frac{4k_p^2}{\Lambda^2}\right) - \frac{3\Lambda^4}{8k_p^4} + \frac{9\Lambda^2}{4k_p^2} - \frac{3\Lambda^3}{k_p^3}\tan^{-1}\left(\frac{2k_p}{\Lambda}\right)\right]\right] \\
&+ \frac{\varepsilon_{ex}^{ul}}{\rho_0}\rho_n\rho_p\left[\frac{3}{32}\left[\left(\frac{\Lambda^6}{k_n^3k_p^3}+\frac{6\Lambda^4}{k_nk_p^3}+\frac{6\Lambda^4}{k_n^3k_p}\right) - \frac{3\Lambda^2(k_p^2-k_n^2)^2}{k_n^3k_p^3}\right]\right] \\
&\times \ln\left[\frac{\Lambda^2+(k_n+k_p)^2}{\Lambda^2+(k_n-k_p)^2}\right] \\
&+ \frac{\varepsilon_{ex}^{ul}}{\rho_0}\rho_n\rho_p\left[\frac{3}{2}\left(\frac{\Lambda^3}{k_n^3}-\frac{\Lambda^3}{k_p^3}\right)\tan^{-1}\left(\frac{k_p-k_n}{\Lambda}\right) - \frac{3}{2}\left(\frac{\Lambda^3}{k_p^3}+\frac{\Lambda^3}{k_n^3}\right)\tan^{-1}\left(\frac{k_n+k_p}{\Lambda}\right)\right] \\
&+ \frac{\varepsilon_{ex}^{ul}}{\rho_0}\rho_n\rho_p\left[\frac{9}{8}\left(\frac{\Lambda^2}{k_p^2}+\frac{\Lambda^2}{k_n^2}\right) - \frac{3}{8}\frac{\Lambda^4}{k_n^2k_p^2}\right]
\end{aligned}
$$

Fitting protocol

- The symmetric nuclear matter (SNM) requires only the following three combinations of the strength parameters,

$$\left(\frac{\varepsilon_0^l + \varepsilon_0^{ul}}{2}\right) = \varepsilon_0, \left(\frac{\varepsilon_\gamma^l + \varepsilon_\gamma^{ul}}{2}\right) = \varepsilon_\gamma, \left(\frac{\varepsilon_{ex}^l + \varepsilon_{ex}^{ul}}{2}\right) = \varepsilon_{ex},$$

  which together with γ, b and α constitute the six parameters for the SNM. For a given value of the exponent γ, which characterizes as the stiffness parameter and determines the incompressibil

- It is demanded that he nuclear mean-field in symmetric nuclear matter at saturation vanished for a kinetic energy of incident nucleaon of 300 MeV. This constraint allows to determine, for a given value of γ, the strength of the excahnege energy, ε_{ex}, and the range of the form factor α.
- The parameter b is determined to avoid the supra-luminous behaviour.
- The two remaining parameters, ε_0 and ε_γ are obtained from given saturation conditions. (density nd energy per baryon)

- The splitting of the exchange strength is decided to be $\varepsilon_{ex}^{l} = 2\varepsilon_{ex}^{ul}/3$, which ensures that the entropy in pure neutron matter does not exceed that of symmetric nuclear matter.
- The splitting of the parameters ε_0 and ε_γ is decided from the value oif the symmetry energy and its slope.
- The characteristic slope of the symmetry energy is fixed from the condition that the asymmetric contribution to the nucleonic part of the energy density in charge neutral beta-stable stellaar matter $npe\mu$ is maximal.
- One of the two free parameters, x_0, is fixed from the spin-up and spin-down splitting of the effective mass in polatized neutron matter.
- Finally the parameter t_0 and the spin-orbit strength W_0 are determined from calculations in finite nuclei.

Landau Parameters

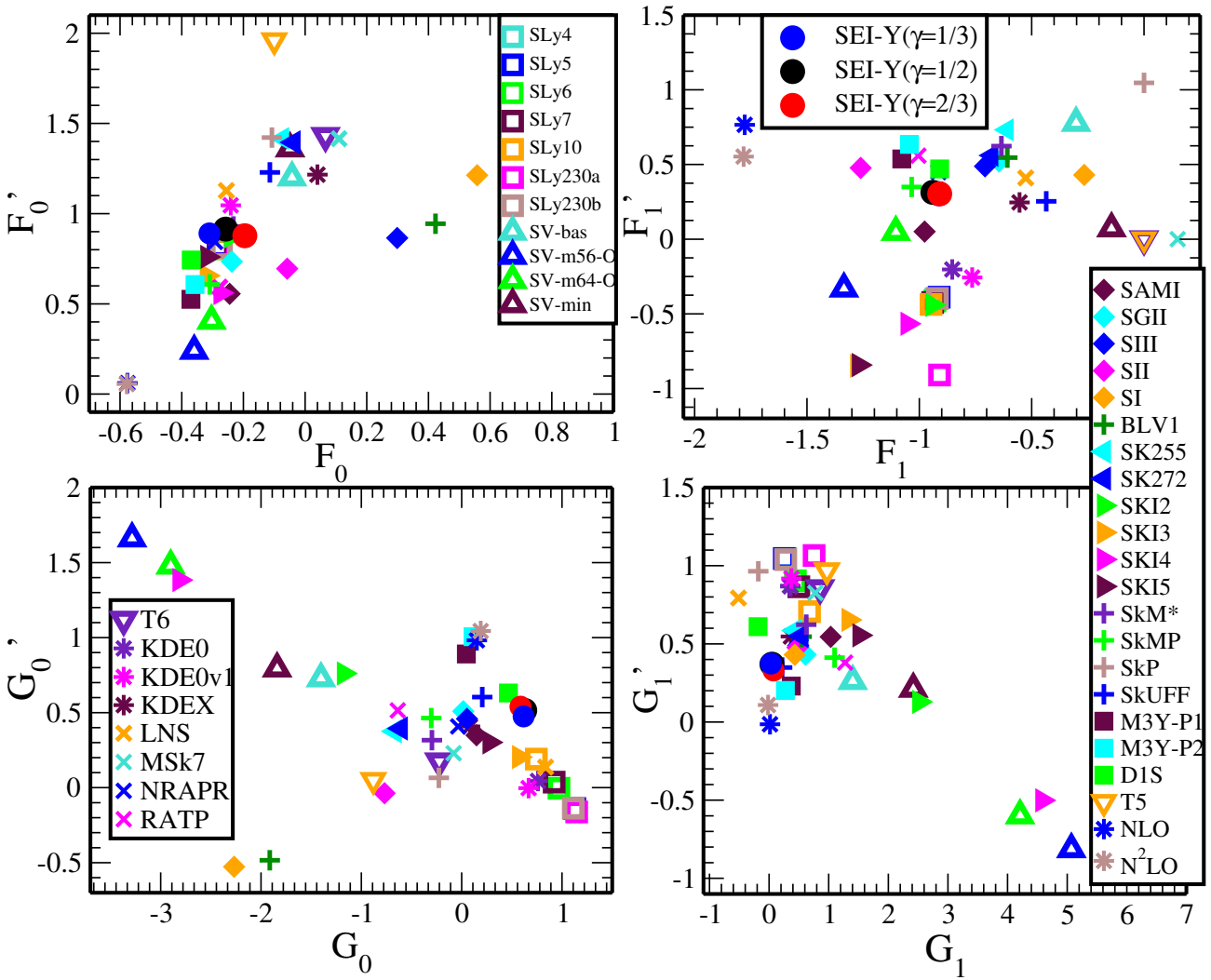

Landau Parameters

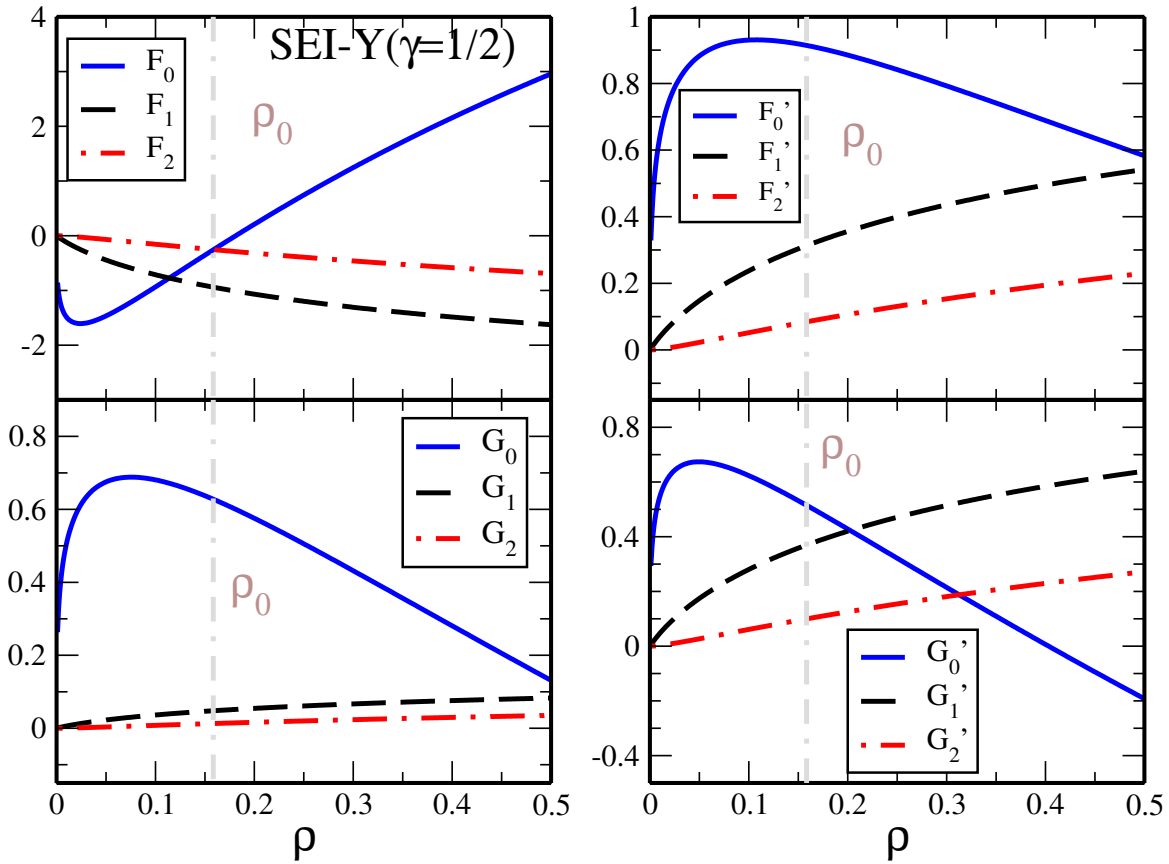

Table: Nuclear matter properties predicted using Landau parameter at saturation density for SEI-Y($\gamma = 1/3$), SEI-Y($\gamma = 1/2$), and SEI-Y($\gamma = 2/3$) sets.

SEI-Y(γ) (γ)	ρ_0 [fm^{-3}]	K_0 [MeV]	$\frac{m_s^*}{m}$	$\frac{m_s^*}{m_v^*}$	E_{sym} [MeV]	E_σ [MeV]	$E_{\sigma\tau}$ [MeV]	mv_s^2 [MeV]
(1/3)	0.161	230.59	0.695	1.101	35.10	30.02	27.38	24.47
(1/2)	0.158	237.74	0.686	1.104	34.048	28.95	26.94	26.38
(2/3)	0.156	263.14	0.696	1.101	34.10	28.79	27.97	27.94

Finite nuclei

$$H = \frac{\hbar^2}{2M}(\tau_0^n + \tau_0^p) + H_{zero} + H_d^{Nucl} + H_{exch,0}^{Nucl} + H_{exch,2}^{Nucl} + H_{SO} + H_{Coul}.$$

$$\begin{aligned} H_{exch,2}^{Nucl}(\vec{R}) &= \sum_q \frac{\hbar^2}{2m}[(f_q - 1)(\tau_q - \frac{3}{5}k_q^2\rho_q - \frac{1}{4}\nabla^2\rho_q) \\ &+ k_q f_q^{'}(\frac{1}{27}\frac{(\nabla\rho_q)^2}{\rho_q} - \frac{1}{36}\nabla^2\rho_q)], \end{aligned}$$

$$h_q\Phi_i = \varepsilon_i\Phi_i$$

where,

$$h_q = -\nabla\frac{\hbar^2}{2m_q^*(\vec{R})}\nabla + U_q(\vec{R}) - iW_q(\vec{R}).[\nabla \times \vec{\sigma}],$$

with

$$\frac{\hbar^2}{2m_q^*(\vec{R})} = \frac{\partial E}{\partial\tau_q(\vec{R})},\ U_q(\vec{R}) = \frac{\partial E}{\partial\rho_q(\vec{R})},\ W_q(\vec{R}) = \frac{\partial E}{\partial\vec{J}_q(\vec{R})}.$$

Spherical nuclei

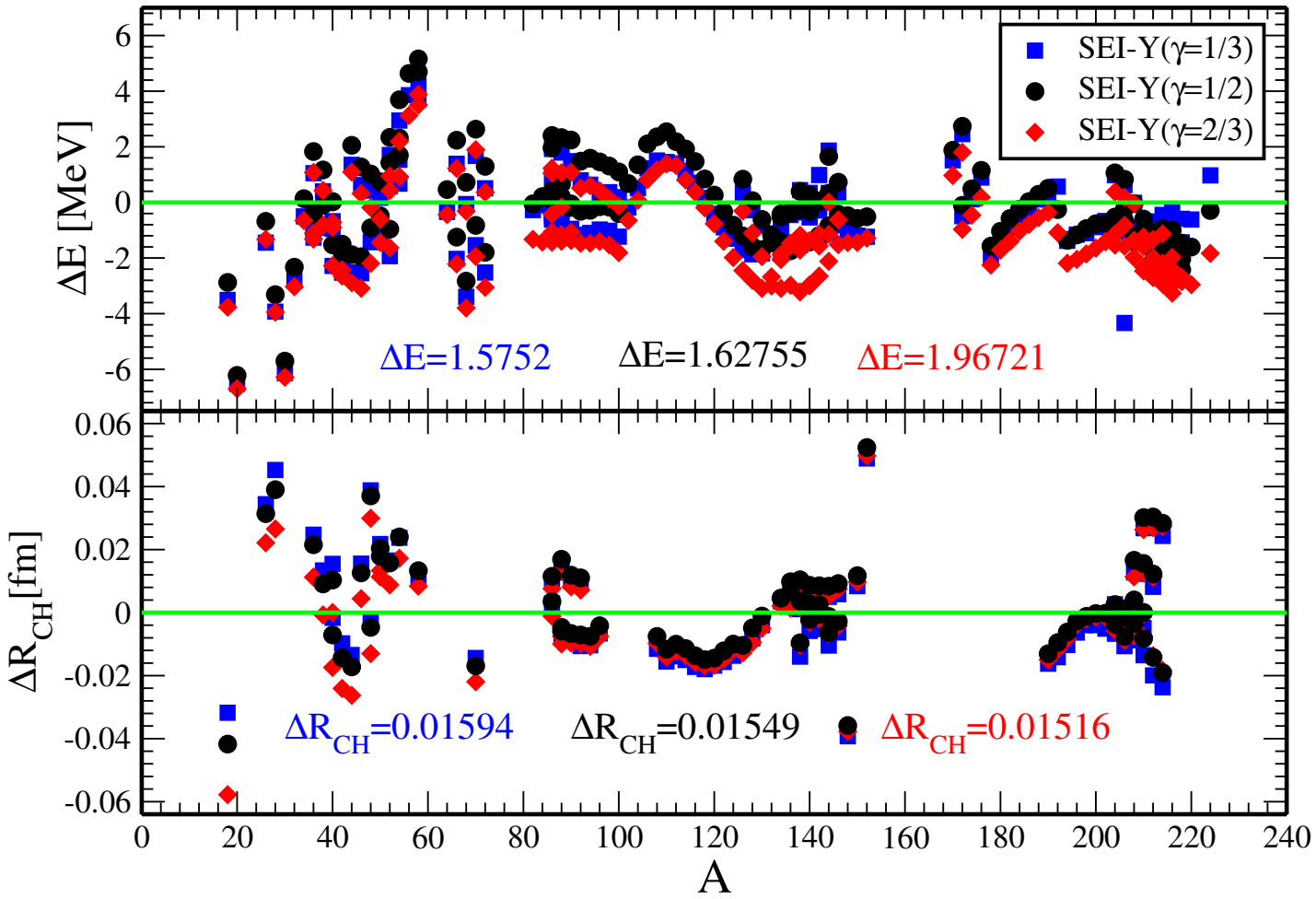

Slope of the incompressibility and Radius of Neutron star

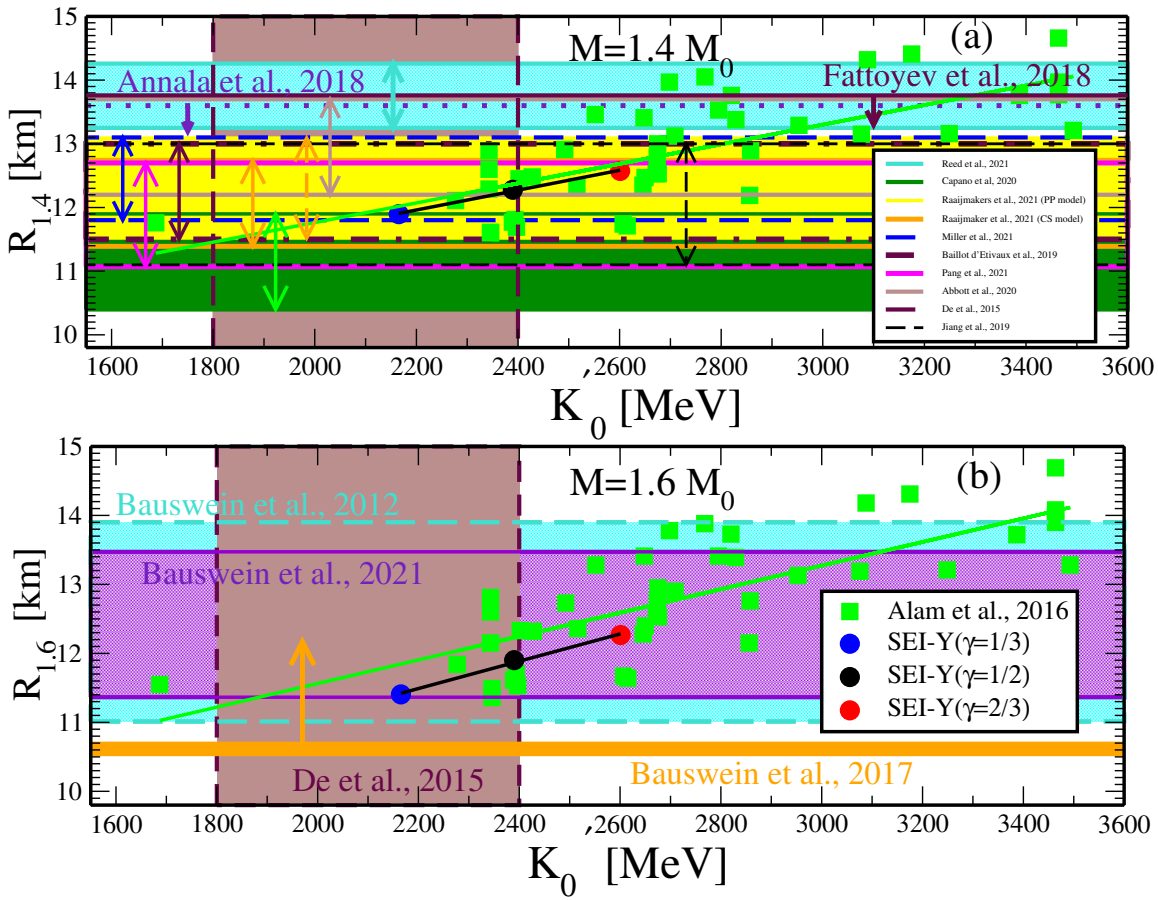

$R_{1.4}$ of 1.4 M_0 neutron stars and (b) Radii $R_{1.6}$ of 1.6 M_0 neutron stars versus the slope of the incompressibility $K_0^{'}$ obtained using different EoS of SEI-Y having γ=1/3, 1/2, and 2/3.

Neutron star merger and incompressibility of ANM

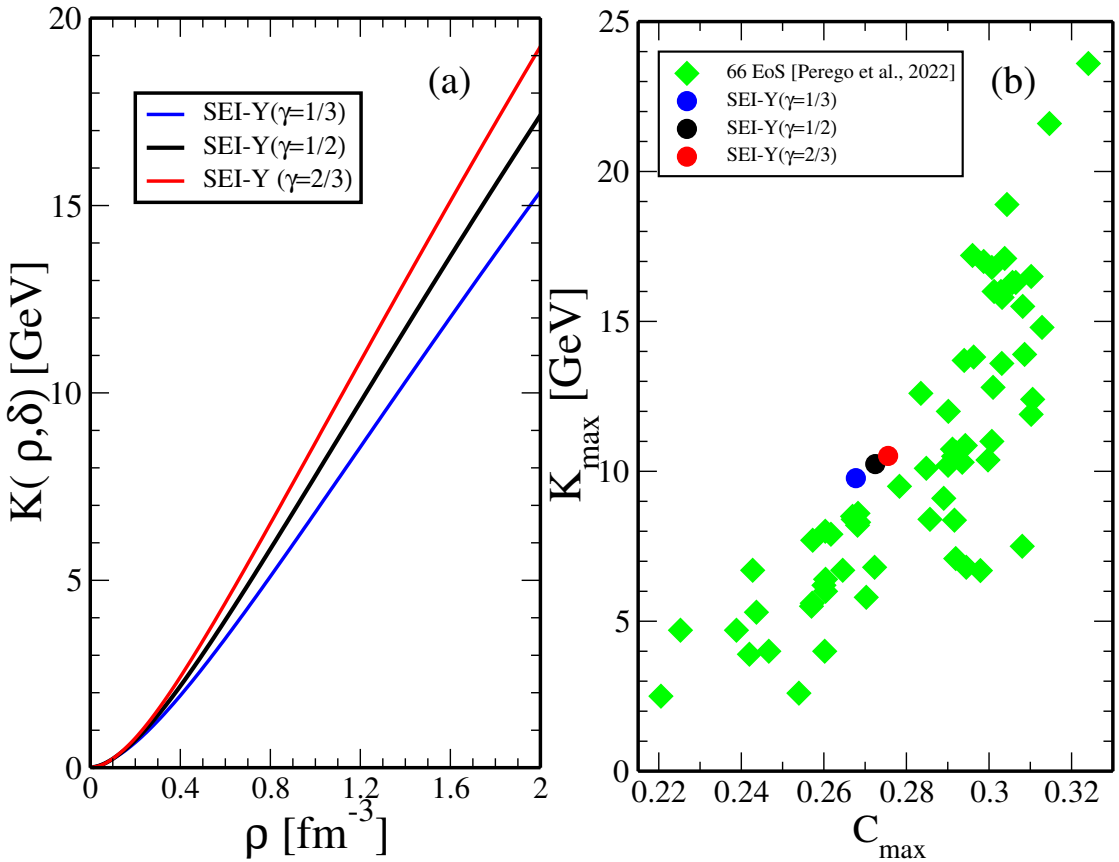

(a) K(ρ, δ) as a function of density in NSM for the SEI-Y$(\gamma = 1/3, 1/2, 2/3)$ EoS, (b) K_{max} as a function of the compactness of the heaviest NS for the three EoS of SEI-Y. Green diamonds are the 66 EoS results taken from A.Perego et al, Phys.Rev.Lett **129**, 032701 (2022).

Sound speed in Neutron Star Matter

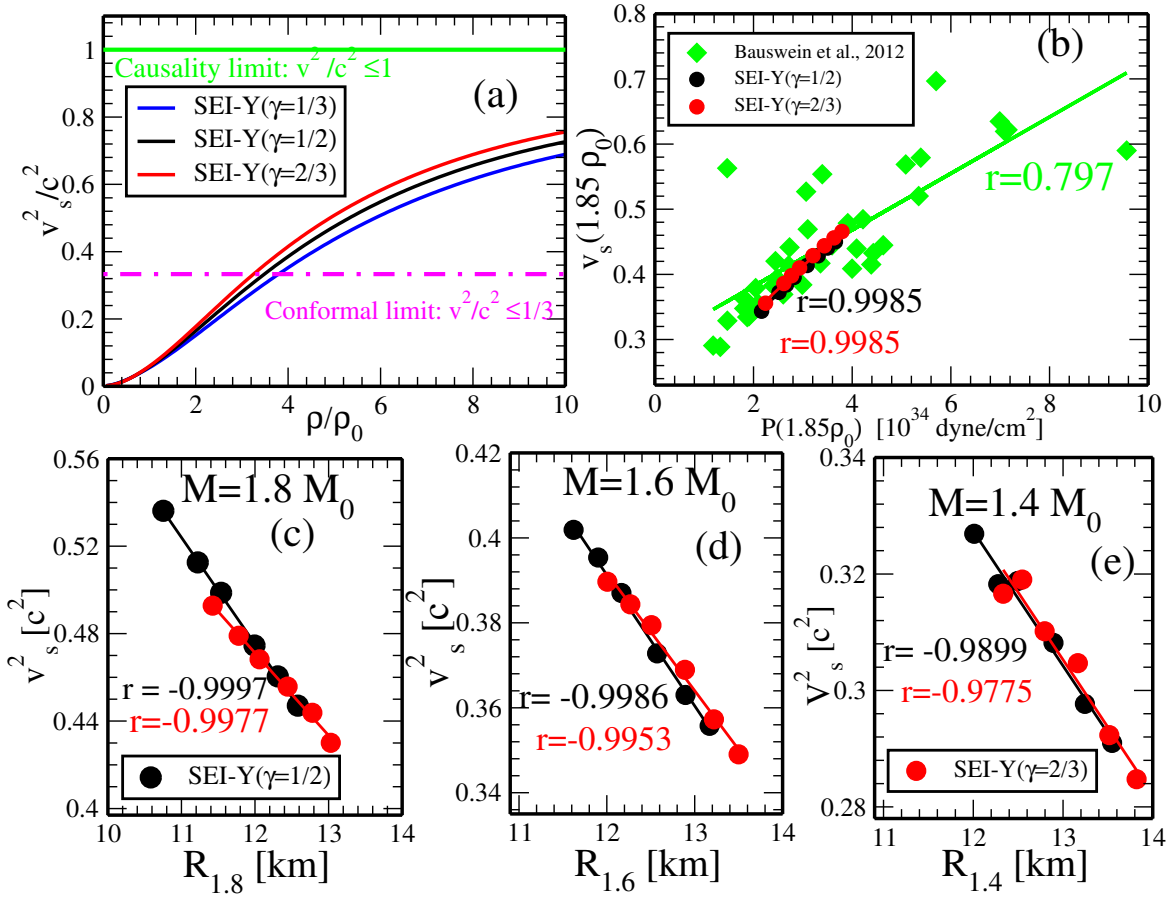

(a) Speed of sound in NSM as a function density for SEI-Y EoS with $\gamma = 1/3, 1/2, 2/3$. (b) At central density $1.85\rho_0$ as a function of pressure. (c)-(e) At central density of different NS as a function its radius. The dots correspond to SEI-Y EoS with slope parameter L in the range 60-110 MeV.

Gravitational redshift (I)

The gravitational redshift of a signal from the star surface is

$$Z_{surf} = \left(1 - \frac{2GM}{c^2 R}\right)^{-1/2} - 1$$

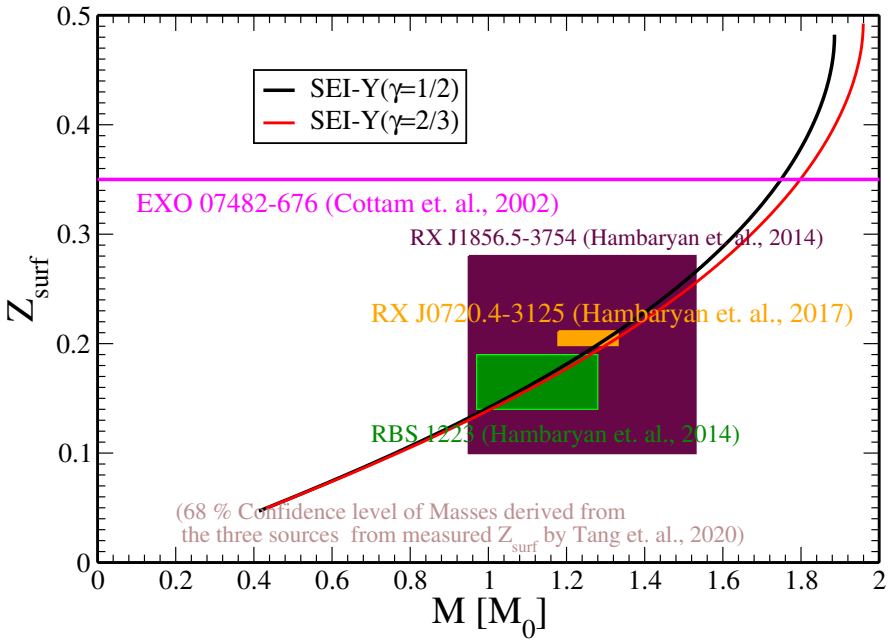

Gravitational redshift at the neutron star surface as a function of the stellar gravitational mass for the SEI-Y ($\gamma = 1/2$) and SEI-Y ($\gamma = 2/3$) EoSs. The extracted ranges for the three NSs, RBS 1223, RX J0720.4-3125, and RX J1856.5-3754 are shown in different shades.

Gravitational redshift (II)

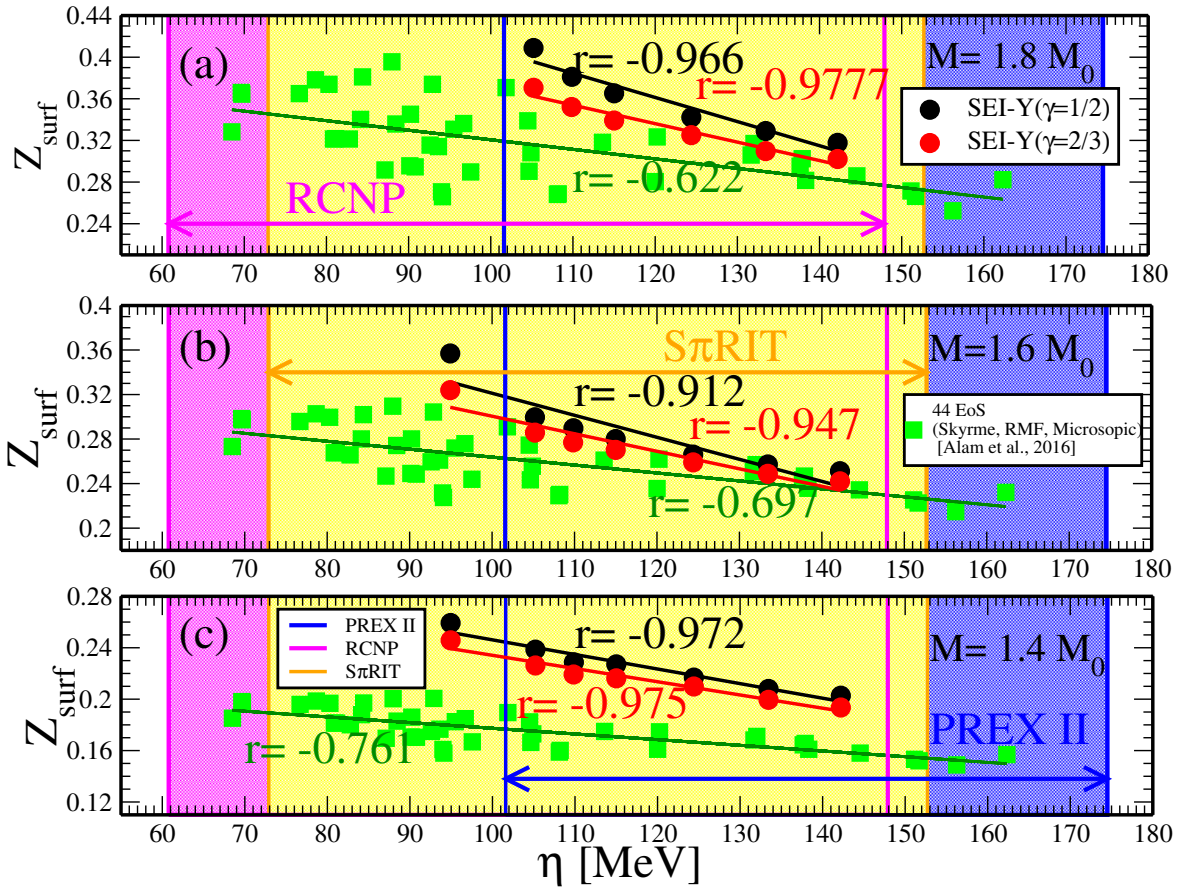

Z_{surf} as a function of η for 1.8 M_0, 1.6 M_0, and 1.4 M_0 NS for SEI-Y ($\gamma = 1/2$) and SEI-Y ($\gamma = 2/3$) EoSs. Shaded region is the constrained value of η for PREX II [Blue], RCNP [magenta], and SπRIT [yellow] [**?**]. The green diamonds are the data for the 44-EoSs of N. Alam et al, Phys.Rev.C94,052801(2016).

Gravitational redshift (III)

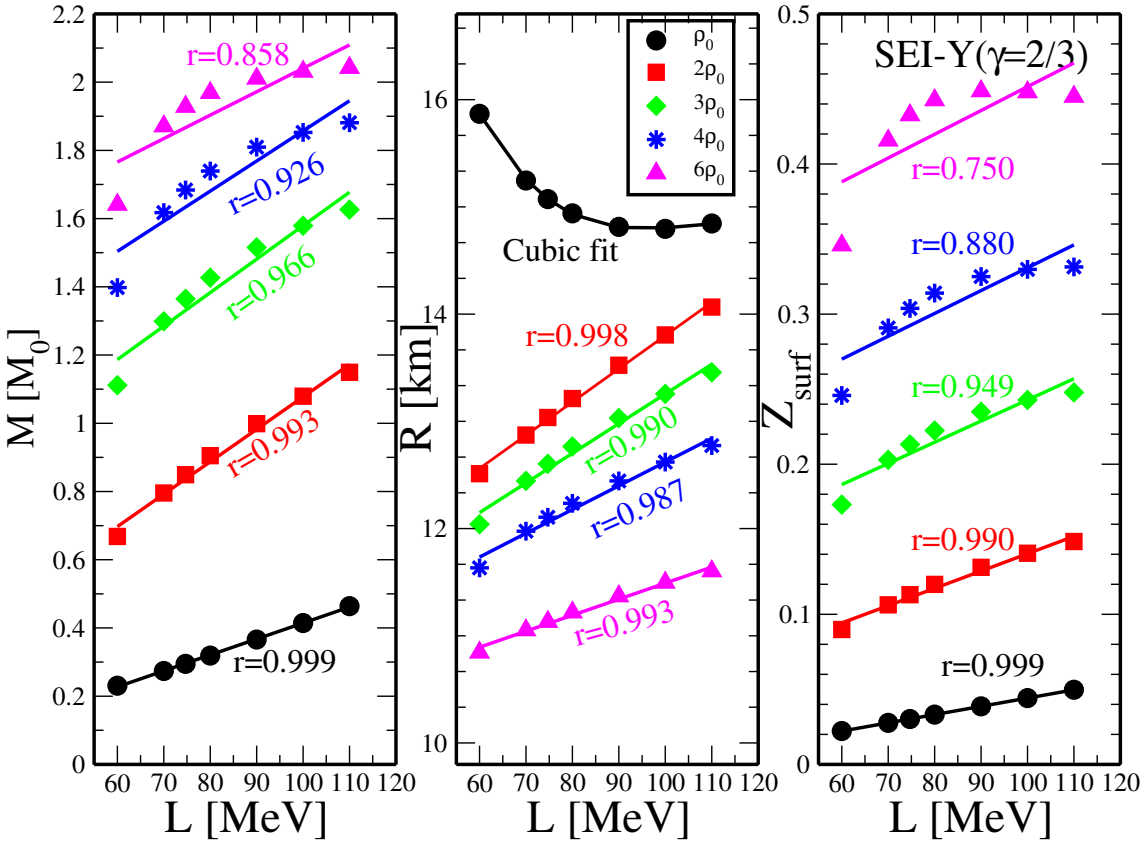

(a) Neutron star masses, (b) Neutron star radius (c) Z_{surf} corresponding to central densities of ρ_0, $2\rho_0$, $3\rho_0$, $4\rho_0$, and $6\rho_0$ as a function of L.